Evolution of the Ultrafast Photoluminescence of Colloidal Silicon Nanocrystals with Changing Surface Chemistry

9 AUTHORS, INCLUDING:

Zhenyu (Kevin) Yang
University of Toronto
27 PUBLICATIONS   201 CITATIONS

SEE PROFILE

Lyubov Titova
Worcester Polytechnic Institute
88 PUBLICATIONS   872 CITATIONS

SEE PROFILE

Jan Linnros
KTH Royal Institute of Technology
69 PUBLICATIONS   1,440 CITATIONS

SEE PROFILE

Jonathan G. C. Veinot
University of Alberta
143 PUBLICATIONS   2,362 CITATIONS

SEE PROFILE

Evolution of the Ultrafast Photoluminescence of Colloidal Silicon Nanocrystals with Changing Surface Chemistry

Zhenyu Yang,[†,‡] Glenda B. De los Reyes,[‡,§] Lyubov V. Titova,[§,∥] Ilya Sychugov,[⊥] Mita Dasog,[†] Jan Linnros,[⊥] Frank A. Hegmann,*[,§] and Jonathan G. C. Veinot*[,†]

[†]Department of Chemistry, University of Alberta, Edmonton, Alberta T6G 2G2, Canada
[§]Department of Physics, University of Alberta, Edmonton, Alberta T6G 2E1, Canada
[⊥]Materials and Nano Physics Department, ICT School, KTH-Royal Institute of Technology, 16440 Kista, Sweden

ⓢ Supporting Information

ABSTRACT: The role of surface species in the optical properties of silicon nanocrystals (SiNCs) is the subject of intense debate. Changes in photoluminescence (PL) energy following hydrosilylation of SiNCs with alkyl-terminated surfaces are most often ascribed to enhanced quantum confinement in the smaller cores of oxidized NCs or to oxygen-induced defect emission. We have investigated the PL properties of alkyl-functionalized SiNCs prepared using two related methods: thermal and photochemical hydrosilylation. Photochemically functionalized SiNCs exhibit higher emission energies than the thermally functionalized equivalent. While microsecond lifetime emission attributed to carrier recombination within the NC core was observed from all samples, much faster, size-independent nanosecond lifetime components were only observed in samples prepared using photochemical hydrosilylation that possessed substantial surface oxidation. In addition, photochemically modified SiNCs exhibit higher absolute photoluminescent quantum yields (AQY), consistent with radiative recombination processes occurring at the oxygen-based defects. Correlating spectrally- and time-resolved PL measurements and XPS-derived relative surface oxidation for NCs prepared using different photoassisted hydrosilylation reaction times provides evidence the PL blue-shift as well as the short-lived PL emission observed for photochemically functionalized SiNCs are related to the relative concentration of oxygen surface defects.

**KEYWORDS:** silicon nanocrystals, photoluminescence, nanosecond lifetime, surface functionalization

Following the discovery of light-emitting porous silicon by Canham,[1] many materials based on nanostructured silicon (e.g., silicon nanocrystals (SiNCs)) have been investigated as candidate active systems for optoelectronics devices, ultrafast data communication, and data storage, as well as fluorescent labels and biological sensors.[2−8] Despite these important practical advances, no clear consensus regarding the origin of optical emission from SiNCs exists.[9−17] Bulk Si does not show efficient luminescence because of its indirect bandgap.[18] However, efficient photoluminescence (PL) from nanostructured silicon has been widely observed; it has been explained in the context of quantum confinement and defect and surface states.[17,19−29]

As expected, PL resulting from the influence of quantum confinement in SiNC cores is size dependent and shifts in the maximum emission energy are inversely proportional to nanocrystal size. In addition, the PL dynamics associated with SiNC core emission range throughout the nanosecond (ns) to microsecond (μs) time scales. Long-lived PL (i.e., μs time scale) observed in the yellow to infrared spectral region is often attributed to quasi-direct[30] and phonon-assisted radiative recombination in the core states of larger SiNCs;[14,31] short-lived blue-green emission (i.e., ns time scale) is often attributed

to quasi-direct recombination in smaller (diameter <2 nm) SiNCs.[11,29,32−35]

Surface chemistry has also been implicated in the PL and emission dynamics of SiNCs.[36] Nanosecond PL in the blue-green and yellow-red spectral regions has been attributed to fast recombination of carriers in surface states (or defects) introduced as a result of ligand passivation and oxidation.[37−43] For blue-emitting alkyl-functionalized SiNCs, charge transfer to surface states has been suggested as one possible mechanism for nanosecond PL decay times.[44−46] For yellow/orange-emitting SiNCs, the origin of similarly short-lifetime PL and a concomitant blue-shifted PL maximum has been attributed to various silicon−oxygen species on the NC surfaces.[15] Contrasting this, suggestions that surface oxidation leads to a decrease in SiNC size that induces a blue-shift of the PL emission maximum have appeared.[47] Complicating the community's understanding, other reports claim surface oxidation induces a red-shift of the PL maximum.[17,33] The authors explained this latter observation by invoking the presence of surface silanones (Si=O) that purportedly introduce new electronic states that lead to "trapped-electron-
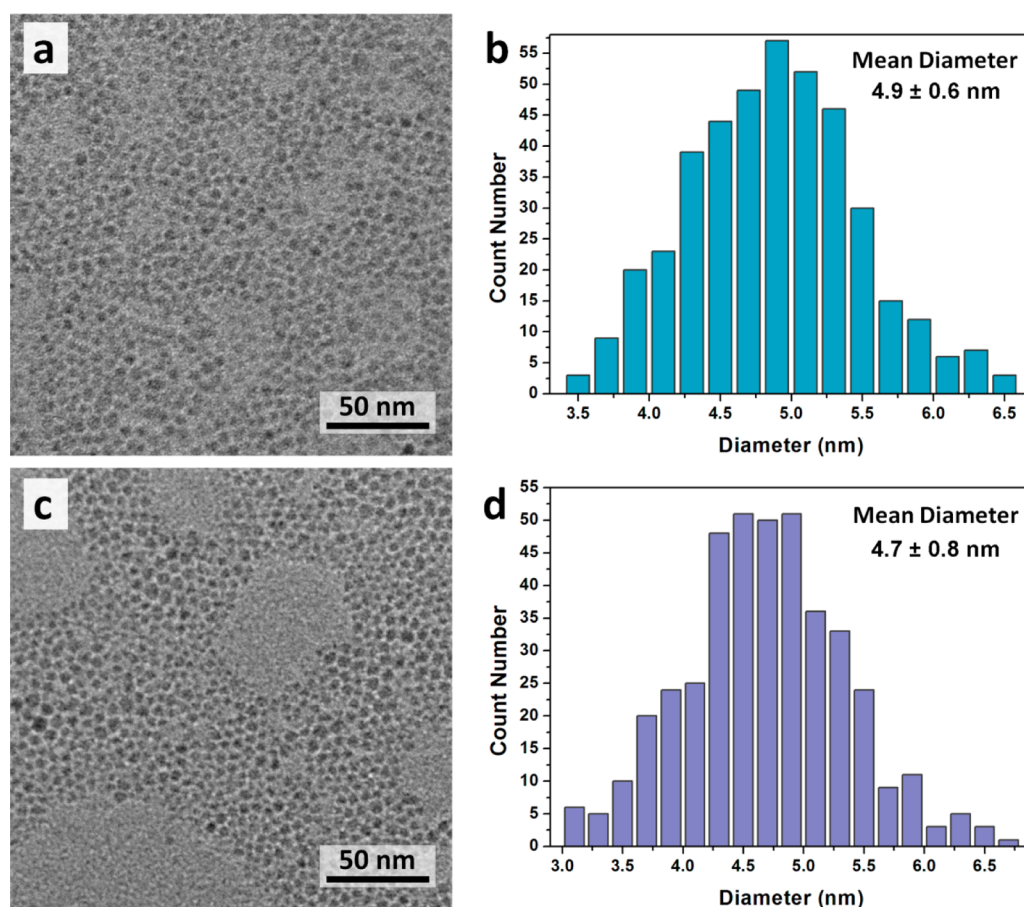
Figure 1. Bright-field TEM images and size distribution of ensembles of 5 nm dodecyl-passivated silicon nanocrystals functionalized via thermal (a, b) and photochemical (c, d) hydrosilylation approaches (reaction time = 15 h).

to-band" recombination. While molecular analogues of the proposed silanone surface groups have been reported, they require substantial stabilization.[48−51] In light of the extreme reactivity of the Si═O moiety and that the stabilization effects of the nanoscale silicon surface cannot be readily predicted, the presence of these species must be considered cautiously. Indeed, nanosecond PL lifetimes observed for alkyl-functionalized and hydride-terminated freestanding yellow/orange emitting SiNCs have been associated with significant surface oxidation.[15,38,41] These seemingly contradicting observations and proposals underscore that the impact of oxygen-containing species on the PL response of SiNCs remains an unresolved issue.[52−54] In this contribution, we investigate the origin of the blue-shift of the PL maximum and nanosecond PL lifetime observed for alkyl-functionalized SiNCs fabricated using two complementary hydrosilylation approaches (i.e., thermal and photochemical initiation). Established differences associated with the efficacy of these closely related functionalization procedures allow for direct comparison of the impact of surface oxide on PL response.

■ RESULTS AND DISCUSSION

Well-defined SiNCs used in the present study were prepared using a well-established procedure developed in the Veinot laboratory.[55] Briefly, commercial hydrogen silsesquioxane was thermally processed in a slightly reducing atmosphere (95% Ar/5% H_2) at 1100 °C (for 3 nm SiNCs) and 1200 °C (for 5 nm SiNCs) to yield well-defined SiNCs embedded in a SiO_2-like matrix. Hydride-terminated SiNCs were freed from the oxide matrix via HF etching. Subsequent surface modification with dodecyl groups was achieved using thermal or photochemical hydrosilylation 1-dodecene. A deep orange solution was obtained after 3 h from thermally induced surface modification. In contrast, even after 15 h of photochemical hydrosilylation, an orange/brown cloudy suspension was observed. This difference in appearance is reasonably attributed to the functionalization of the NC surfaces during thermal hydrosilylation that render them compatible with organic solvents and less efficient surface passivation being achieved via the photochemically initiated reaction (vide infra). Transmission electron microscope (TEM) imaging and corresponding size distributions (Figures 1 and S1) of the dodecyl-functionalized SiNCs indicate NCs modified using these two procedures possess near identical, statistically equivalent dimensions.

Fourier transform infrared (FTIR) spectra of 5 and 3 nm SiNCs are shown in Figures 2a and S2a, respectively. Freshly etched hydride-terminated SiNCs exhibit two distinct absorptions that are confidently attributed to Si−H$_x$ stretching and scissoring (i.e., 2000−2100 and 900 cm^{-1}). Following hydrosilylation with 1-dodecene, the Si−H$_x$ features are replaced by intense vibrations at 2650−2900 and 1380−1470 cm^{-1}, indicative of C−H stretching and bending vibrations of dodecyl surface moieties. Consistent with other studies,[56−58] we note Si−O−Si stretching features at about 1100 cm^{-1}, indicative of some surface oxidation. A straightforward comparison of the
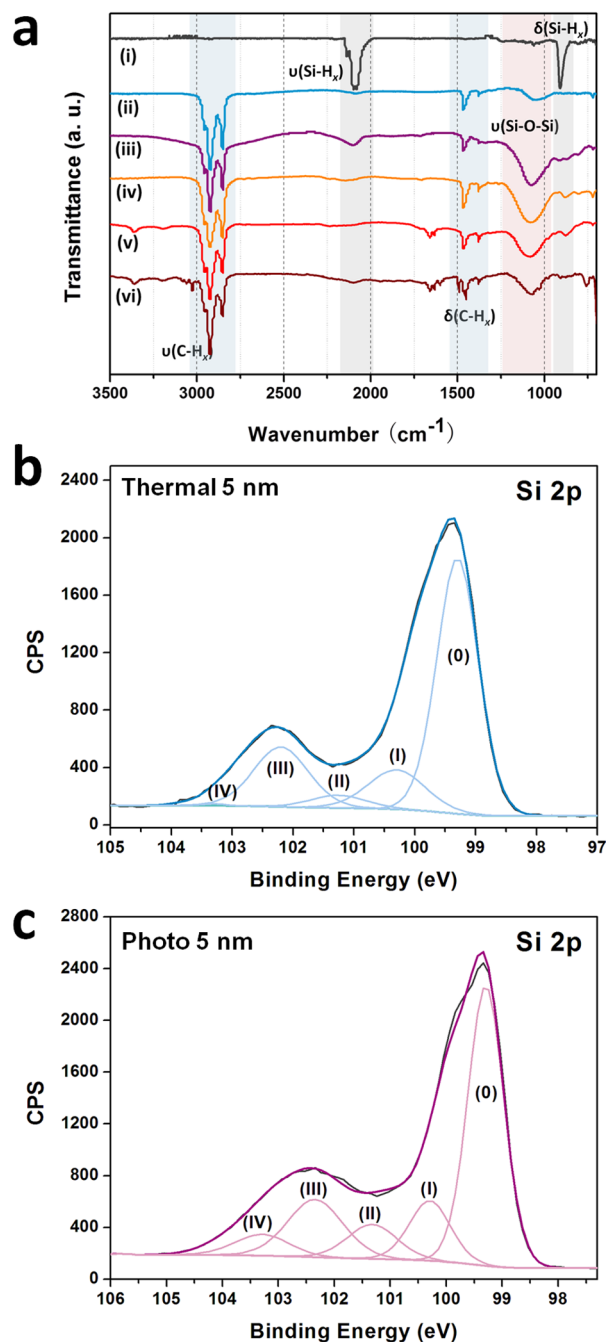
Figure 2. (a) FTIR spectra of hydride-terminated (i) thermally functionalized (ii) photochemically functionalized d = 5 nm SiNCs (reaction time = 15 (iii), 20 (iv), 30 (v), and 39 h (vi)). (b, c) High-resolution XP spectra of the Si 2p spectral region for SiNC (diameter = 5 nm) corresponding to SiNCs whose FTIR spectra are in panels (ii) and (iii). Fits are shown for the Si $2p_{3/2}$ emissions. Si $2p_{1/2}$ components have been omitted for clarity.

FTIR spectra suggests the surfaces of photochemically functionalized SiNCs consistently bear more Si−O species than their thermally modified equivalents.[59]

X-ray photoelectron spectroscopy (XPS) is commonly used to gain insight into the nature (i.e., speciation and quantity) of surface oxidation on alkyl-functionalized SiNCs.[28,31,60,61] All spectra (see Figures 2 and S2) confirm only Si, C, and O are present in the SiNC samples studied here. The Si 2p spectral region of the high-resolution XP spectrum of the thermally and

photochemically modified 5 nm diameter particles are shown in Figure 2b and c, respectively. The emission feature at 99.3 eV arises from the Si(0) core of the SiNCs.[61] The broad feature between about 100 and 104 eV is routinely fit to components at 100.3 (Si(I)), 101.4 (Si(II)), and 102.4 (Si(III)) arising from ligand functionalized surface and Si suboxides; an additional component at 103.4 eV (Si(IV)) is consistent with SiO_2.[28,61−64] Consistent with FTIR analyses (vide supra), spectral features attributable to surface oxides appear for thermally and photochemically modified samples, and the oxide features, in particular, the significant Si(IV) emission, are more intense for photochemically functionalized samples. Of important note, the XP spectrum of thermally modified 5 nm SiNCs is similar to that of its 3 nm counterpart (Figure S2), however, the contribution of Si(IV) species is smaller in the former. In contrast, the photochemically modified 5 nm SiNCs showed the highest relative content of Si(IV) of all samples evaluated here.

Figure 3a,b shows the time-integrated PL of surface-modified SiNCs (d = 3 and 5 nm) excited by 400 nm laser pulses at a fluence of 77 $\mu J/cm^2$. The time-integrated PL maxima are summarized in Figure 4. Regardless of the functionalization method employed, increasing the NC size from 3 to 5 nm induces a red-shift of the PL maximum (i.e., 49 nm for thermal and 88 nm for 15 h photochemical), suggestive of quantum confinement. All samples exhibit broad PL spectra with Gaussian-like profiles. The line widths of the PL arising from thermally modified SiNCs are broader than their photo-chemical counterparts. The origin of the observed broadening of SiNC PL is complex. While some broadening may arise from the distribution of particle sizes present in the sample (i.e., as a result of quantum confinement), single dot spectroscopy studies of individual SiNCs also show broad emission spectra.[65,66]

A comparison of the optical response shows the PL maximum of photochemically functionalized SiNCs (Figure 3b) is blue-shifted from that of analogous thermally function-alized SiNCs (Figure 3a). As noted above (Figures 1 and S1), TEM analyses of the samples indicate there is no statistically relevant difference in their sizes. However, a qualitative inspection of the TEM size distributions suggests the PL may be influenced by a biasing of the particle size distribution that may result from the established size-dependent reactivity of photochemical hydrosilylation.[59] To explore this possibility, the SiNC diameter corresponding to the PL peak emission was calculated using the effective mass approximation (EMA):[67−69]

$$E_g^{opt} = E_g + \frac{\hbar^2\pi^2}{2R^2\mu} - \frac{1.786e^2}{\varepsilon_r R} \quad (1)$$

$$\mu = \frac{m_e^* m_h^*}{m_h^* + m_e^*}$$

where E_g is the band gap of bulk silicon (1.12 eV), R is the nanocrystal radius, e is the electronic charge, ε_r is the relative permittivity (for silicon, ε_r = 11.68), m_e^* and m_h^* are the effective masses of the electrons and holes (0.19m_0 and 0.286m_0, respectively, where m_0 is the free electron rest mass),[28] and μ is the reduced mass. From eq 1, it is evident that a PL maximum of 815 nm (i.e., PL observed here for d = 5 nm SiNCs modified using thermally induced hydrosilylation) corresponds to a diameter of 4.1 nm; a PL maximum of 726 nm ((i.e., PL observed here for d = 5 nm SiNCs modified via a
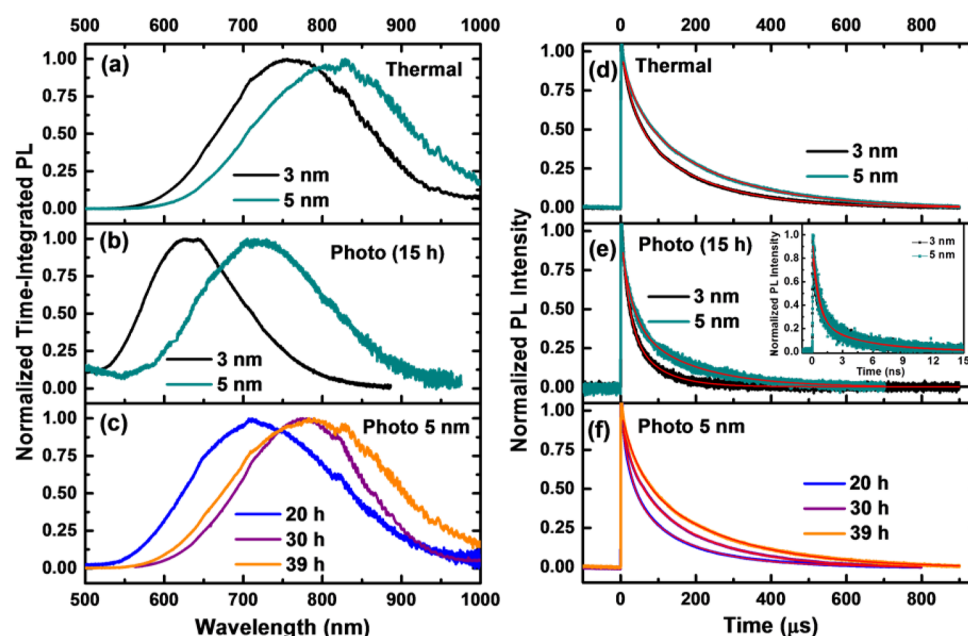
Figure 3. Time-integrated PL spectra of surface functionalized SiNCs prepared using (a) thermal and (b) photochemical hydrosilylation. (c) Reaction time dependence of PL arising from photochemically modified SiNCs ($d = 5$ nm) upon excitation by $\lambda = 400$ nm laser pulses at 77 μJ/cm^2 fluence. Corresponding time-resolved PL decays are shown in panels (d), (e), and (f), respectively. The inset in panel (e) shows the nanosecond lifetime PL emission at 630 and 690 nm for 3 and 5 nm SiNCs, respectively. Solid red lines are fits to the PL decay.
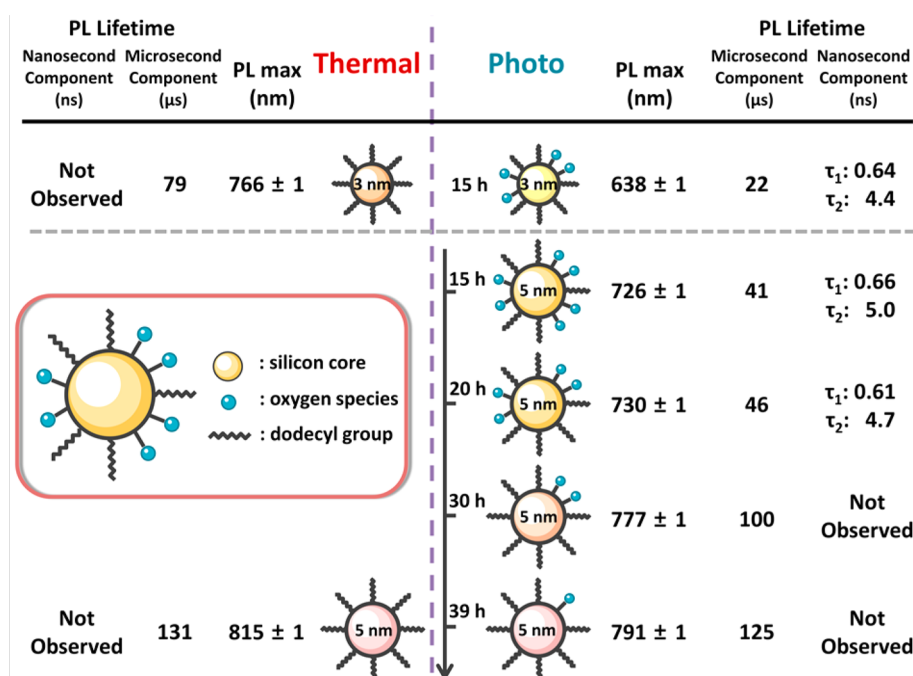
Figure 4. Summary of time-integrated PL maxima and time-resolved PL lifetimes for surface functionalized SiNCs.

15 h photochemically induced hydrosilylation) corresponds to a diameter of 3.3 nm. Based upon these calculated diameters and the presented TEM data, it is possible the PL from thermally functionalized SiNCs has a strong contribution from a significant number (~24%) of particles with diameters ≤4.1 nm. Fewer particles (~4.8%) with diameters ≤3.3 nm are present in photochemically functionalized SiNCs. Therefore, it is unlikely that the observed blue-shift of the time-integrated PL is due to excitation of these small particles alone. However, Biteen et al. reported that surface oxidation led to a decrease in NC size, which resulted in an observed PL blue-shift.[47] For the

present study, even though the FTIR and XPS analyses show more surface oxide is present in photochemically modified SiNCs, close examination of the TEM images shown in Figure 1 affords no evidence of such a size reduction. In this context, it is reasonable that any size reduction of the SiNC core arising from surface oxidation is negligible.

Emission from oxidized porous silicon is normally comprised of two components, a slow yellow-orange-red band and a fast band in the blue-green region.[70,71] It has been proposed that the slow band region originates from quantum core-states of SiNCs and has a characteristic decay of a few tens to a few

hundreds of microseconds. The fast band emission has been attributed to oxygen-induced defects or charge transfer states and decays in the nanosecond range.[10,15,40,72] If the blue-shifted PL arising from photochemically modified SiNCs arises from excitation of smaller nanocrystals and emission from defect sites, then both ns and μs PL emission decay components are expected.

To test this hypothesis, the PL emission dynamics of all the samples presented here were explored (see Figures 3 and S5–S8). The μs-PL decays represent the overall time decay for the entire emission spectrum. The ns-component of the decay time was measured at particular emission wavelengths. The carrier recombination dynamics of the ns-PL component is biexponential according to

$$y(t) = Ae^{-t/\tau_1} + Be^{-t/\tau_2} + C \tag{2}$$

where τ_1 and τ_2 are the decay times and C is a constant offset much smaller than A and B. The μs-PL component exhibits a stretched exponential decay:

$$y(t) = Ae^{(-t/\tau)^\beta} + y_0 \tag{3}$$

where τ is the decay time, β is the dispersion factor, and y_0 is a constant offset. The carrier recombination lifetime values are summarized in Figures 4 and 5.

The photoexcited state lifetime of $d = 3$ nm SiNCs modified using thermally induced hydrosilylation is $\tau = 78.6 \pm 0.1$ μs; this is similar to previously reported values for SiNCs and is attributed to recombination within the Si(0) core.[14,26,73] For the same size of photochemically modified SiNCs, the μs-component was notably faster ($\tau = 22.0 \pm 0.3$ μs) and exhibited a ns-component with $\tau_1 = 0.64$ ns and $\tau_2 = 4.4$ ns at 630 nm (see Figure 3e, inset). Unlike the μs-PL component, the ns PL exhibits a double exponential decay as clearly shown in the semilog plot in Figure S4. It is important to note that no ns-lifetime component is observed for thermally functionalized SiNCs (Figure S5). For a given hydrosilylation method, the measured PL dynamics for 5 nm diameter SiNCs is similar to that observed for analogous 3 nm diameter SiNCs. The μs component for the $d = 5$ nm thermally modified SiNCs showed a decay time of $\tau = 130.5 \pm 0.1$ μs; nanosecond and microsecond lifetimes coexist for 5 nm diameter SiNCs that were photochemically functionalized (Figures 5 and S7). The μs-PL decay times for the 5 nm diameter SiNCs are longer than those for the 3 nm diameter SiNCs, consistent with previous studies.[13,14,67]

Multiexponential decay behavior in the nano and microsecond ranges have also been reported for colloidal SiNCs dispersed in chloroform[74] and hexane,[75] as well as SiNCs embedded in an SiO$_2$ matrix.[10] Unlike the ns decays commonly reported for blue/blue-green-emitting SiNCs, the ns-PL components observed here for photochemically modified SiNCs occur at wavelengths commonly associated with "slow band" emission (yellow-red) (see Figures S6 and S7). Kim et al. observed similar ns-PL decay times from freshly etched freestanding SiNCs with an emission maximum at 657 nm.[15] They proposed the blue-shift of the PL maximum and reduction in carrier recombination lifetime from 49.9 μs to ~3 ns after removing the SiO$_2$ matrix was associated with oxide and interface defects arising from surface oxidation. In our case, surface oxides are present in thermally and photochemically functionalized SiNCs (vide supra). However, XPS and FTIR data indicate the photochemically modified SiNCs have
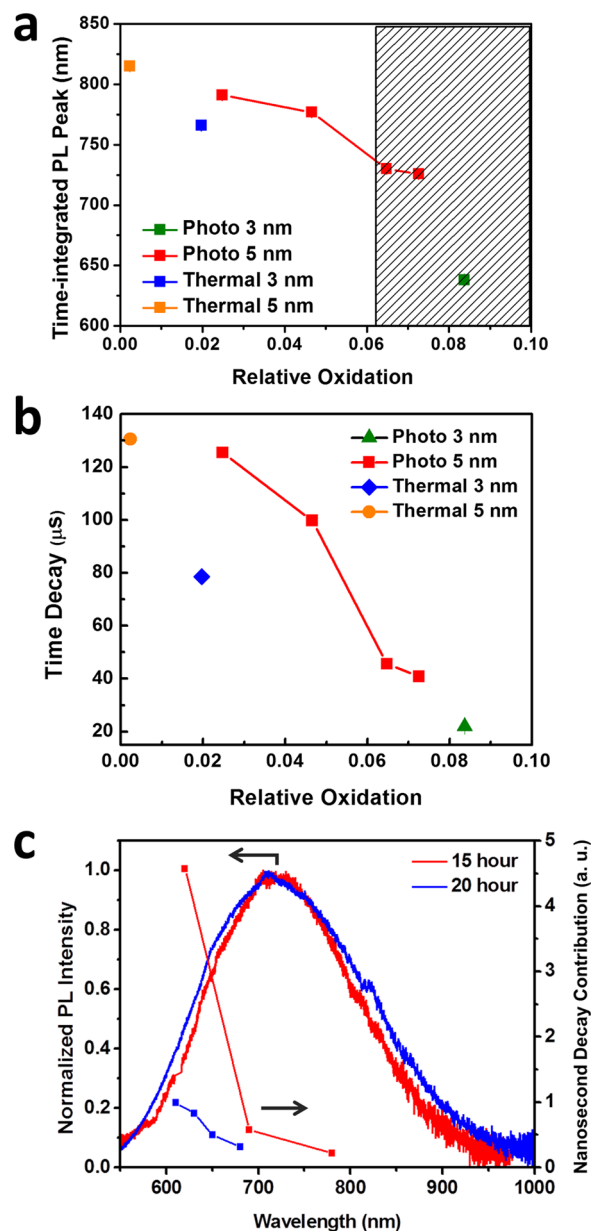
Figure 5. (a) Maxima of time-integrated PL spectra and (b) microsecond PL lifetime components for SiNCs prepared using thermal and photochemical hydrosilylation as a function of XPS-derived relative surface oxidation. The shaded area in (a) corresponds to the relative oxidation region in which nanosecond and microsecond PL lifetimes coexist. (c) Time-integrated PL spectra for 5 nm photochemically functionalized SiNCs with reaction times of 15 and 20 h. The corresponding magnitude of the spectrally resolved nanosecond PL decay contribution is also shown.

substantially more silicon oxide and that the speciation of oxides differs significantly for the two surface functionalization methods (vide supra). We propose the blue-shift of the PL maximum as well as the existence of ns-lifetime components for photochemically modified SiNCs is related to differences (i.e., quantity and speciation) in the surface oxidation. Although the PL emission shifts to lower energy when the size is increased, the general trend of the PL lifetime decay of these 5 nm samples is similar to that of the 3 nm samples for a given hydrosilylation method. The stark similarities (i.e., quantity and speciation) of the oxide species determined by FTIR and XPS,

as well as the PL dynamics, strongly suggest the origin of the ns lifetime is the same for the 3 and 5 nm SiNCs prepared using 15 h photochemical hydrosilylation. In addition, the decay time of the μs-PL component from the 15 h photochemically modified SiNCs is significantly less than that observed for their thermally modified counterparts. This observation suggests the μs-PL component observed from photochemically functionalized SiNCs is dominated by emission from smaller NCs within the distribution (vide infra). All these results support the initial hypothesis that the observed PL blue-shift in photochemically modified SiNCs can be attributed to the emission from smaller NCs in addition to emission from oxygen-induced defects.

Consistent with reports related to different hydrosilylation reactions on silicon surfaces,[59,76] we contend the limited reaction time (i.e., 15 h) used for photochemical hydrosilylation led to incomplete surface functionalization. Surface oxidation may also occur during purification. Furthermore, it is reasonable that prolonging the photochemical modification procedure would provide a more complete passivation of the SiNC surfaces and allow for indirect tailoring of the amount of surface oxidation resulting from the workup procedures.[76−78] To investigate this possibility, a series of time-dependent photochemical hydrosilylation experiments were performed. Herein, d = 5 nm SiNCs were chosen as the model because their comparatively slow photochemical hydrosilylation provides a larger range of surface passivation. FTIR spectra of SiNCs after prolonged photochemical hydrosilylation show a less intense Si−O−Si stretching absorption consistent with less surface oxidation and supporting our hypothesis (Figure 2a). To provide a semiquantitative measure of the degree of SiNC surface oxidation as a function of photochemical hydrosilylation reaction time, we estimated the relative oxidation purely based on the Si(IV) contribution in the Si 2p region of the XP spectra. This was achieved by normalizing the area under Si(IV) component to total area of the entire Si 2p emission. We intentionally neglected suboxide contributions because their exact chemical identity was not straightforward to elucidate. As shown in Figure S9, the XPS-derived relative oxidation decreases with prolonged reaction time. It is reasonable this trend results from more complete surface passivation/functionalization with longer reaction times. Concurrently, the intensities of signals arising from silicon suboxides (i.e., Si(I), Si(II), and Si(III)) increase slightly, consistent with the proposal that more hydride terminated Si surface sites have been modified by alkyl ligands (Figure S3).

Figure 3c shows the time-integrated PL spectra of photochemically modified SiNCs after functionalization for the indicated reaction times; the evolution of the PL emission maximum is summarized in Figure 4. The PL arising from the 20 h sample is centered at about 730 nm. Extending the reaction time to 30 h induced an obvious red-shift to about 777 nm. The magnitude of the red-shift continues to increase with increased reaction time and after 39 h, the PL maximum of SiNCs centers at about 791 nm, close to the 815 nm PL peak obtained for SiNCs prepared using thermal hydrosilylation. Moreover, the samples obtained after a 15 h photochemical reaction are cloudy, while the solution of SiNCs after 39 h was completely transparent, similar to the thermally prepared SiNCs. These results support the proposal that longer photochemical reaction times lead to more complete surface functionalization.

To explore the impact of surface oxidation on the PL emission dynamics of the present surface functionalized SiNCs, the time-integrated PL maximum and microsecond decay component were plotted as a function of XPS-derived relative oxidation. Figure 5a,b shows that, as the relative oxidation increases, the time-integrated PL maximum shifts to higher energy, while the decay time of the μs-PL component decreases. Again, we assert this shift of PL maximum to higher energy does not arise from an oxygen-induced reduction in NC size (vide supra). A reasonable explanation for this behavior is an increase in the number of luminescent defect centers associated with increased surface oxidation. Based on literature accounts, carrier trapping at defect sites occurs very rapidly and can dominate, if not totally quench, core-state related emission.[79−82] Oxygen-induced-defect quenching of the PL is more likely observed in larger NCs within an ensemble since they are functionalized more slowly and therefore have more surface oxides than smaller NCs.[59] As a result, the PL from the larger SiNCs is quenched more than that from smaller NCs, contributing to the observed PL blue-shift, consistent with computational studies.[83,84] This explains the decrease in decay time of the μs-PL component with increased relative oxidation. The AQY measurements of the 3 nm SiNCs show photochemically functionalized SiNCs exhibit a comparatively higher AQY (66 ± 8%) than its thermal counterpart (AQY = 41 ± 3%). This result suggests oxygen moieties at the NC surface are not nonradiative because the AQY is higher for the more oxidized NCs. From this we conclude surface oxygen moieties are radiative centers and that the measured ns decay is a radiative process. It is important to note that both thermal and photochemical hydrosilylation resulted in partial surface oxidation, however, the ns component was only detected at comparatively high surface oxidation levels. It is possible that the PL of thermally functionalized SiNCs has ns components as well, but because the surface oxidation is present in much lower quantities, the ns signal is below the detection limit of our system. Based on AQY and PL dynamics measurements, it is likely that the observed blue-shift of PL maximum arises from a combination of emission from smaller NCs and from oxygen-induced surface defect sites.

Figure 5a,b shows the time-integrated PL peak and μs PL lifetime as a function of relative oxidation. The shaded area in Figure 5a corresponds to the relative oxidation region where both ns- and μs-PL components were observed. It is evident that, regardless of NC size, an increase in surface oxidation leads to a blue-shift of PL maximum accompanied by a short-lived ns-PL component. This result is consistent with the assumption that the ns-PL component is associated with the increase of defect sites as the relative surface oxidation increases. Contrary to other reports,[33] we conclude from the present data (i.e., Figures S6 and S7) that oxygen-defect-related PL may occur at energies higher than the core-states.[10]

Figure 5c shows the relative amplitude of the ns-PL component of the 15 and 20 h photochemically functionalized SiNCs. The observed increase in the amplitude of the ns-PL component at higher energies affirms the hypothesis that carrier radiative recombination at oxygen-induced defects contributes to the PL blue-shift. A similar result was observed for 3 nm photochemically functionalized SiNCs (Figure S10). Based on our hypothesis, if the PL blue-shift is minimized/eliminated by ensuring complete surface passivation, the defect-related ns-PL component should be suppressed and ultimately disappears if a prolonged photochemical reaction is employed. Indeed, this is

the case for the present reaction time-dependent experiments (Figures 4 and S9). All samples exhibit μs-PL components, while ns-PL components were only detected for samples obtained from shorter photochemical reaction times (i.e., 15 and 20 h, shown in Figure 3c). In addition, the 39 h photochemically functionalized SiNCs exhibit PL emission dynamics very similar to that of the thermally functionalized SiNCs.

■ CONCLUSIONS

The interconnection between SiNC size-independent PL blue-shift, nanosecond excited-state lifetime and XPS-derived relative oxidation has been examined and confirmed through systematic investigations of dodecyl-functionalized SiNCs. Differences in the effectiveness of thermal and photochemical hydrosilylation methods to passivate SiNC surfaces provide an opportunity to control the degree of surface modification on alkyl-terminated SiNCs and by extension of surface oxidation. PL emission maxima arising from SiNCs functionalized using 15 h photochemical hydrosilylation (both 3 and 5 nm) are significantly blue-shifted compared to their thermal counter-parts. The difference in emission energies cannot be solely attributed to quantum confinement effects because the difference in average diameters and size distributions is small, if not negligible. A microsecond PL lifetime component was observed for all samples, regardless of functionalization methodology, and has been attributed to SiNC core state radiative recombination. Size-independent nanosecond lifetime components (<7 ns) were only observed for samples prepared using the photochemical approach that exhibit substantial relative surface oxidation. Time-dependent experiments indicate that the observed blue-shift of PL maxima and nanosecond lifetime in photochemically modified SiNCs are related to the degree of surface oxidation resulting from incomplete functionalization of the SiNC surface.

■ EXPERIMENTAL SECTION

Reagents and Materials. Hydrogen silsesquioxane (HSQ) was purchased from Dow Corning Corporation (Midland, MI) as FOx-17. Electronics grade hydrofluoric acid (HF, 49% aqueous solution) was purchased from J. T. Baker. Reagent grade methanol, toluene, and ethanol, as well as 1-dodecene (97%), were purchased from Sigma-Aldrich and used as received. Dry toluene was prepared by adding sodium pieces and benzophenone indicator, refluxing for 24 h, and finally obtained from an Ar-filled still system.

Synthesis and Liberation of SiNCs. *Preparation of Oxide-Embedded SiNCs (d = 3 nm).* Established literature procedures were used to prepare oxide-embedded silicon nanocrystals (SiNC/SiO$_2$).[56] Briefly, solvent was removed from the stock HSQ solution (FOx-17) under vacuum to yield a white solid. The solid (ca. 4 g) was placed in a quartz reaction boat and transferred to a Lindberg Blue tube furnace and heated from ambient to a peak processing temperature of 1100 °C at 18 °C min^{-1} in a slightly reducing atmosphere (5% H$_2$/95% Ar). The sample was maintained at the peak processing temperature for 1 h. Upon cooling to room temperature, the resulting amber solid was ground into a fine brown powder using a two-step process. The solid was crushed using an agate mortar and pestle to remove large particles and finally ground to a fine powder using a Burrell Wrist Action Shaker upon shaking with high-purity silica beads for 5 h. The

resulting SiNC/SiO$_2$ powders were stable for extended periods and stored in standard glass vials.

Preparation of Oxide-Embedded SiNCs (d = 5 nm). After grinding with a mortar and pestle (vide supra), 0.5 g of SiNC/SiO$_2$ composite containing 3 nm SiNCs were transferred to a high temperature furnace (Sentro Tech Corp.) for further thermal processing in an inert argon atmosphere. This procedure leads to particle growth while maintaining relatively narrow particle size distributions. In the furnace, the SiNC/SiO$_2$ composite was heated to 1200 °C at 10 °C/min to achieve the target particle size. Samples were maintained at the peak processing temperature for 1 h. After cooling to room temperature, the brown composites were ground using procedures identical to those noted above.

Liberation of SiNCs. Hydride-terminated SiNCs were liberated from the SiNC/SiO$_2$ composite by HF etching. A total of 0.25 g of ground Si-NC/SiO$_2$ composite were transferred to a polyethylene terephthalate beaker equipped with a Teflon coated stir bar. Ethanol (3 mL) and water (3 mL) were added under mechanical stirring to form a brown suspension followed by 3 mL of 49% HF aqueous solution (**Caution!** HF must be handled with extreme care). After 1 h of etching in subdued light, the suspension appeared orange/yellow. Hydride-terminated SiNCs were subsequently extracted from the aqueous layer into about 30 mL of toluene by multiple (i.e., 3 × 10 mL) extractions. The SiNC toluene suspension was transferred to test tubes and the SiNCs were isolated by centrifugation at 3000 rpm.

Thermal and Photochemical Hydrosilylation Approaches. *Formation of 3 and 5 nm Dodecyl-Functionalized SiNCs (Thermal Hydrosilylation).* After decanting the toluene supernatant, the resulting hydride-terminated particles were redispersed into about 20 mL of dodecene to yield a cloudy suspension that was transferred to a dry 100 mL Schlenk flask equipped with a magnetic stir bar and attached to an argon-charged Schlenk line. The flask was evacuated and backfilled with argon three times. The Schlenk flask was placed in an oil bath, and the temperature was increased to 190 °C. The reaction was stirred at peak temperature for a minimum of 15 h, yielding a transparent orange/yellow solution.

Formation of 3 and 5 nm Dodecyl-Functionalized SiNCs (Photochemical Hydrosilylation). After centrifugation at 3000 rpm for 5 min, the toluene supernatant was decanted and the precipitated hydride-terminated SiNCs were redispersed into dry toluene. The solution was recentrifuged at 3000 rpm for another 5 min. Again, the toluene supernatant was decanted and particles were redispersed into dodecene: dry toluene mixture (7.5 mL of dodecene and 30 mL toluene). The mixture was transferred into a predried Schlenk flask equipped with a stir bar and quartz insert for photochemical reaction under an argon atmosphere. The reaction mixtures were subjected to three freeze−pump−thaw cycles, and photochemical hydro-silylation was carried out using a 365 nm UV LED light source for 15 h. For the functionalization time-dependent study, 5 nm hydride-terminated SiNCs were chosen for model experiments. The UV initiated hydrosilylation reaction mixtures were processed for predefined times (i.e., 20, 30, and 39 h).

Purification of SiNCs. Following thermal and photo-chemical hydrosilylation, reaction mixtures were equally distributed among 1.5 mL centrifuge tubes (ca. 0.3 mL each) and about 1.2 mL of 1:1 methanol/ethanol mixture was added to each tube to yield a cloudy yellow dispersion. The precipitate was isolated by centrifugation in a high-speed centrifuge at

17000 rpm for 15 min. The supernatant was decanted and the particles were redispersed in a minimum amount of toluene and subsequently precipitated by addition of the 1:1 methanol–water again. Centrifugation and decanting procedure was repeated twice. Finally, the purified functionalized Si-NCs were redispersed in toluene, filtered through a 0.45 μm PTFE syringe filter, and stored in vials for further use.

Material Characterization and Instrumentation. FTIR spectroscopy was performed on powder samples using a Nicolet Magna 750 IR spectrophotometer. X-ray photoelectron spectroscopy (XPS) measurements were acquired in energy spectrum mode at 210W, using a Kratos Axis Ultra X-ray photoelectron spectrometer. Samples were prepared as film drop-cast from solution onto a copper foil substrate. CasaXPS software (VAMAS) was used to interpret high-resolution spectra. All of the spectra were internally calibrated to the C 1s emission (284.8 eV). Transmission electron microscopy (TEM) and energy dispersive X-ray (EDX) analyses were performed using a JEOL-2010 (LaB$_6$ filament) electron microscope with an accelerating voltage of 200 keV. High resolution TEM (HRTEM) imaging was performed on JEOL-2200FS TEM instrument with an accelerating voltage of 200 kV. TEM and HRTEM samples of SiNCs were drop-casted onto a holey carbon coated copper grid and allowing the solvent to evaporate under vacuum. TEM and HRTEM images were processed using ImageJ software (version 1.45).

For optical measurements, dodecyl-functionalized SiNC were dissolved in toluene and filtered to yield transparent solutions and placed in a quartz cuvette for PL and PL lifetime measurements. The samples were excited by 400 nm second harmonic signal from a BBO crystal pumped by 800 nm pulses from Ti:sapphire laser (RegA900, 65 fs pulse width and 250 kHz repetition rate). The average excitation power was 1.83 mW. Time-integrated PL spectra were recorded using a thermoelectric-cooled CCD (Acton Pixis 400B, Princeton Instruments) coupled to a spectrometer (Acton SP2500, Princeton Instruments). A 435 nm long pass filter (Edmund optics) was placed at the entrance of the spectrometer to block scattered light from the excitation laser pulses. PL spectra were integrated for 120 s. Nanosecond PL lifetime was recorded using a single-photon avalanche photodiode (SPAD, PDM Series by Micro Photon Devices) coupled to a time-correlated single-photon counting (TCSPC) unit (Picoharp 300, Picoquant) with a time resolution of 54 $\pm$ 1 ps. For microsecond carrier recombination lifetime measurements, 1 kHz frequency-doubled 400 nm pulses from another Ti:sapphire laser (Legend Elite, 45 fs pulse width) were used to excite PL at an average excitation power of 4.5 mW. A fast silicon photodiode (Thorlabs, PDA36A rise time 20.6 ns) coupled to a 300 MHz oscilloscope (Tektronix) was used. The photodiode was placed on a path perpendicular to the excitation beam and 10 nm bandpass filters (Edmund Optics) were used to select a particular emission wavelength.

Quantum yield measurements were carried out in a home-built system consisting of a laser-driven Xenon plasma white-light source (Energetic) with a wavelength-selecting mono-chromator for the excitation, a 6" integrating sphere (Lab-sphere), and a thermoelectrically cooled CCD camera after spectrometer (Prinston Instruments) for the detection. The sample solutions were placed in Suprasil quartz cuvettes and a cuvette with a pure solvent (toluene) was used as a reference. Before the measurements, the system response curve was evaluated for the same positions of the spectrometer grating as for actual measurements using the same light source calibrated with an optical power meter. Obtained spectra for the sample and the reference solutions were corrected for system response and subtracted from each other. Then the absolute QY was found as the ratio between the number of absorbed and emitted photons, evaluated by integrating resulting excitation and luminescence peaks, respectively.

■ ASSOCIATED CONTENT

Ⓢ Supporting Information
Transmission electron microscopy images, FTIR spectra, XPS, and wavelength-dependent PL dynamics of 3 nm functionalized SiNCs, and time-dependent photochemical hydrosilylation results. The Supporting Information is available free of charge on the ACS Publications website at DOI: 10.1021/ac-sphotonics.5b00143.

■ AUTHOR INFORMATION

Corresponding Authors
*E-mail: hegmann@ualberta.ca.
*E-mail: jveinot@ualberta.ca.
Present Address
∥Department of Physics, Worcester Polytechnic Institute, Worcester, Massachusetts 01609, United States.
Author Contributions
‡These authors contributed equally (Z.Y. and G.B.D.l.R.).
Notes
The authors declare no competing financial interest.

■ REFERENCES

(1) Canham, L. T. Silicon Quantum Wire Array Fabrication by Electrochemical and Chemical Dissolution of Wafers. *Appl. Phys. Lett.* **1990**, *57*, 1046.
(2) Alsharif, N. H.; Berger, C. E. M.; Varanasi, S. S.; Chao, Y.; Horrocks, B. R.; Datta, H. K. Alkyl-Capped Silicon Nanocrystals Lack Cytotoxicity and have Enhanced Intracellular Accumulation in Malignant Cells via Cholesterol-Dependent Endocytosis. *Small* **2009**, *5*, 221.
(3) Erogbogbo, F.; Yong, K.-T.; Roy, I.; Xu, G.; Prasad, P. N.; Swihart, M. T. Biocompatible Luminescent Silicon Quantum Dots for Imaging of Cancer Cells. *ACS Nano* **2008**, *2*, 873.
(4) Park, J.-H.; Gu, L.; von Maltzahn, G.; Ruoslahti, E.; Bhatia, S. N.; Sailor, M. J. Biodegradable Luminescent Porous Silicon Nanoparticles for In Vivo Applications. *Nat. Mater.* **2009**, *8*, 331.

(5) Pavesi, L.; Dal Negro, L.; Mazzoleni, C.; Franzo, G.; Priolo, F. Optical Gain in Silicon Nanocrystals. *Nature* **2000**, *408*, 440.

(6) Holman, Z. C.; Liu, C.-Y.; Kortshagen, U. R. Germanium and Silicon Nanocrystal Thin-Film Field-Effect Transistors from Solution. *Nano Lett.* **2010**, *10*, 2661.

(7) Liu, C.-Y.; Holman, Z. C.; Kortshagen, U. R. Hybrid Solar Cells from P3HT and Silicon Nanocrystals. *Nano Lett.* **2008**, *9*, 449.

(8) Barbagiovanni, E. G.; Lockwood, D. J.; Simpson, P. J.; Goncharova, L. V. Quantum Confinement in Si and Ge Nanostructures: Theory and Experiment. *Appl. Phys. Rev.* **2014**, *1*, 011302-1−011302-47.

(9) Sung, K.; Yong Min, P.; Suk-Ho, C.; Kyung Joong, K.; Dong Hoon, C. Temperature-Dependent Carrier Recombination Processes in Nanocrystalline Si/SiO$_2$ Multilayers Studied by Continuous-Wave and Time-Resolved Photoluminescence. *J. Phys. D: Appl. Phys.* **2007**, *40*, 1339.

(10) de Boer, W. D. A. M.; Timmerman, D.; Dohnalova, K.; Yassievich, I. N.; Zhang, H.; Buma, W. J.; Gregorkiewicz, T. Red Spectral Shift and Enhanced Quantum Efficiency in Phonon-Free Photoluminescence from Silicon Nanocrystals. *Nat. Nanotechnol.* **2010**, *5*, 878.

(11) Kanemitsu, Y. Luminescence Properties of Nanometer-Sized Si Crystallites: Core and Surface States. *Phys. Rev. B* **1994**, *49*, 16845.

(12) Kovalev, D. I.; Yaroshetzkii, I. D.; Muschik, T.; Petrova-Koch, V.; Koch, F. Fast and Slow Visible Luminescence Bands of Oxidized Porous Si. *Appl. Phys. Lett.* **1994**, *64*, 214.

(13) Fan, J. C.; Chen, C. H.; Chen, Y. F. Observation of Persistent Photoluminescence in Porous Silicon: Evidence of Surface Emission. *Appl. Phys. Lett.* **1998**, *72*, 1605.

(14) Garcia, C.; Garrido, B.; Pellegrino, P.; Ferre, R.; Moreno, J. A.; Morante, J. R.; Pavesi, L.; Cazzanelli, M. Size Dependence of Lifetime and Absorption Cross Section of Si Nanocrystals Embedded in SiO$_2$. *Appl. Phys. Lett.* **2003**, *82*, 1595.

(15) Kim, S.; Shin, D. H.; Choi, S.-H. Ultrafast Photoluminescence from Freestanding Si Nanocrystals. *Appl. Phys. Lett.* **2012**, *100*, 253103.

(16) Žídek, K.; Pelant, I.; Trojánek, F.; Malý, P.; Gilliot, P.; Hönerlage, B.; Oberlé, J.; Šiller, L.; Little, R.; Horrocks, B. R. Ultrafast Stimulated Emission Due to Quasidirect Transitions in Silicon Nanocrystals. *Phys. Rev. B* **2011**, *84*, 085321.

(17) Wolkin, M. V.; Jorne, J.; Fauchet, P. M.; Allan, G.; Delerue, C. Electronic States and Luminescence in Porous Silicon Quantum Dots: The Role of Oxygen. *Phys. Rev. Lett.* **1999**, *82*, 197.

(18) Alex, V.; Finkbeiner, S.; Weber, J. Temperature Dependence of the Indirect Energy Gap in Crystalline Silicon. *J. Appl. Phys.* **1996**, *79*, 6943.

(19) English, D. S.; Pell, L. E.; Yu, Z.; Barbara, P. F.; Korgel, B. A. Size Tunable Visible Luminescence from Individual Organic Monolayer Stabilized Silicon Nanocrystal Quantum Dots. *Nano Lett.* **2002**, *2*, 681.

(20) Dohnalová, K.; Ondič, L.; Kůsová, K.; Pelant, I.; Rehspringer, J. L.; Mafouana, R.-R. White-Emitting Oxidized Silicon Nanocrystals: Discontinuity in Spectral Development with Reducing Size. *J. Appl. Phys.* **2010**, *107*, 053102.

(21) Dohnalová, K.; Kůsová, K.; Cibulka, O.; Ondič, L.; Pelant, I. Time-Resolved Measurements of Optical Gain and Photoluminescence in Silicon Nanocrystals. *Phys. Scr.* **2010**, *2010*, 014011.

(22) Valenta, J.; Fucikova, A.; Vácha, F.; Adamec, F.; Humpolíčková, J.; Hof, M.; Pelant, I.; Kůsová, K.; Dohnalová, K.; Linnros, J. Light-Emission Performance of Silicon Nanocrystals Deduced from Single Quantum Dot Spectroscopy. *Adv. Funct. Mater.* **2008**, *18*, 2666.

(23) Voos, M.; Uzan, P.; Delalande, C.; Bastard, G.; Halimaoui, A. Visible Photoluminescence from Porous Silicon: A Quantum Confinement Effect Mainly Due to Holes? *Appl. Phys. Lett.* **1992**, *61*, 1213.

(24) Fauchet, P. M. Photoluminescence and Electroluminescence from Porous Silicon. *J. Lumin.* **1996**, *70*, 294.

(25) Ledoux, G.; Gong, J.; Huisken, F.; Guillois, O.; Reynaud, C. Photoluminescence of Size-Separated Silicon Nanocrystals: Confirmation of Quantum Confinement. *Appl. Phys. Lett.* **2002**, *80*, 4834.

(26) Littau, K. A.; Szajowski, P. J.; Muller, A. J.; Kortan, A. R.; Brus, L. E. A Luminescent Silicon Nanocrystal Colloid via a High-Temperature Aerosol Reaction. *J. Phys. Chem.* **1993**, *97*, 1224.

(27) Warner, J. H.; Rubinsztein-Dunlop, H.; Tilley, R. D. Surface Morphology Dependent Photoluminescence from Colloidal Silicon Nanocrystals. *J. Phys. Chem. B* **2005**, *109*, 19064.

(28) Hessel, C. M.; Reid, D.; Panthani, M. G.; Rasch, M. R.; Goodfellow, B. W.; Wei, J.; Fujii, H.; Akhavan, V.; Korgel, B. A. Synthesis of Ligand-Stabilized Silicon Nanocrystals with Size-Dependent Photoluminescence Spanning Visible to Near-Infrared Wavelengths. *Chem. Mater.* **2011**, *24*, 393.

(29) Valenta, J.; Fucikova, A.; Pelant, I.; Kůsová, K.; Dohnalová, K.; Aleknavičius, A.; Cibulka, O.; Fojtík, A.; Kada, G. On the Origin of the Fast Photoluminescence Band in Small Silicon Nanoparticles. *New J. Phys.* **2008**, *10*, 073022.

(30) Sychugov, I.; Valenta, J.; Mitsuishi, K.; Fujii, M.; Linnros, J. Photoluminescence Measurements of Zero-Phonon Optical Transitions in Silicon Nanocrystals. *Phys. Rev. B* **2011**, *84*, 125326.

(31) Mastronardi, M. L.; Maier-Flaig, F.; Faulkner, D.; Henderson, E. J.; Kübel, C.; Lemmer, U.; Ozin, G. A. Size-Dependent Absolute Quantum Yields for Size-Separated Colloidally-Stable Silicon Nanocrystals. *Nano Lett.* **2011**, *12*, 337.

(32) Wilcoxon, J. P.; Samara, G. A.; Provencio, P. N. Optical and Electronic Properties of Si Nanoclusters Synthesized in Inverse Micelles. *Phys. Rev. B* **1999**, *60*, 2704.

(33) Dohnalova, K.; Poddubny, A. N.; Prokofiev, A. A.; de Boer, W. D. A. M.; Umesh, C. P.; Paulusse, J. M. J.; Zuilhof, H.; Gregorkiewicz, T. Surface Brightens up Si Quantum Dots: Direct Bandgap-Like Size-Tunable Emission. *Light. Sci. Appl.* **2013**, *2*, e47.

(34) Sankaran, R. M.; Holunga, D.; Flagan, R. C.; Giapis, K. P. Synthesis of Blue Luminescent Si Nanoparticles Using Atmospheric-Pressure Microdischarges. *Nano Lett.* **2005**, *5*, 537.

(35) Zhou, Z.; Brus, L.; Friesner, R. Electronic Structure and Luminescence of 1.1 and 1.4 nm Silicon Nanocrystals: Oxide Shell versus Hydrogen Passivation. *Nano Lett.* **2003**, *3*, 163.

(36) Dohnalová, K.; Gregorkiewicz, T.; Kůsová, K. Silicon Quantum Dots: Surface Matters. *J. Phys.: Condens. Matter* **2014**, *26*, 173201.

(37) Dohnalová, K.; Žídek, K.; Ondič, L.; Kůsová, K.; Cibulka, O.; Pelant, I. Optical Gain at the F-Band of Oxidized Silicon Nanocrystals. *J. Phys. D: Appl. Phys.* **2009**, *42*, 135102.

(38) Tsybeskov, L.; Vandyshev, J. V.; Fauchet, P. M. Blue Emission in Porous Silicon: Oxygen-Related Photoluminescence. *Phys. Rev. B* **1994**, *49*, 7821.

(39) Gole, J. L.; Dudel, F. P.; Grantier, D.; Dixon, D. A. Origin of Porous Silicon Photoluminescence: Evidence for a Surface Bound Oxyhydride-Like Emitter. *Phys. Rev. B* **1997**, *56*, 2137.

(40) Pi, X. D.; Liptak, R. W.; Nowak, J. D.; Wells, N. P.; Carter, C. B.; Campbell, S. A.; Kortshagen, U. Air-Stable Full-Visible-Spectrum Emission from Silicon Nanocrystals Synthesized by an All-Gas-Phase Plasma Approach. *Nanotechnology* **2008**, *19*, 245603.

(41) Augustine, B. H.; Irene, E. A.; He, Y. J.; Price, K. J.; McNeil, L. E.; Christensen, K. N.; Maher, D. M. Visible Light Emission from Thin Films Containing Si, O, N, and H. *J. Appl. Phys.* **1995**, *78*, 4020.

(42) Rosso-Vasic, M.; Spruijt, E.; Popovic, Z.; Overgaag, K.; van Lagen, B.; Grandidier, B.; Vanmaekelbergh, D.; Dominguez-Gutierrez, D.; De Cola, L.; Zuilhof, H. Amine-Terminated Silicon Nanoparticles: Synthesis, Optical Properties and Their Use in Bioimaging. *J. Mater. Chem.* **2009**, *19*, 5926.

(43) Kůsová, K.; Cibulka, O.; Dohnalová, K.; Pelant, I.; Valenta, J.; Fučíková, A.; Žídek, K.; Lang, J.; Englich, J.; Matějka, P.; Štěpánek, P.; Bakardjieva, S. Brightly Luminescent Organically Capped Silicon Nanocrystals Fabricated at Room Temperature and Atmospheric Pressure. *ACS Nano* **2010**, *4*, 4495.

(44) Dasog, M.; Yang, Z.; Regli, S.; Atkins, T. M.; Faramus, A.; Singh, M. P.; Muthuswamy, E.; Kauzlarich, S. M.; Tilley, R. D.; Veinot, J. G. C. Chemical Insight into the Origin of Red and Blue Photoluminescence Arising from Freestanding Silicon Nanocrystals. *ACS Nano* **2013**, *7*, 2676.

(45) Wolf, O.; Dasog, M.; Yang, Z.; Balberg, I.; Veinot, J. G. C.; Millo, O. Doping and Quantum Confinement Effects in Single Si Nanocrystals Observed by Scanning Tunneling Spectroscopy. *Nano Lett.* **2013**, *13*, 2516.

(46) Dasog, M.; De los Reyes, G. B.; Titova, L. V.; Hegmann, F. A.; Veinot, J. G. C. Size versus Surface: Tuning the Photoluminescence of Freestanding Silicon Nanocrystals Across the Visible Spectrum via Surface Groups. *ACS Nano* **2014**, *8* (9), 9636.

(47) Biteen, J. S.; Lewis, N. S.; Atwater, H. A.; Polman, A. Size-Dependent Oxygen-Related Electronic States in Silicon Nanocrystals. *Appl. Phys. Lett.* **2004**, *84*, 5389.

(48) Xiong, Y.; Yao, S.; Driess, M. An Isolable NHC-Supported Silanone. *J. Am. Chem. Soc.* **2009**, *131*, 7562.

(49) Xiong, Y.; Yao, S.; Müller, R.; Kaupp, M.; Driess, M. From Silicon(II)-Based Dioxygen Activation to Adducts of Elusive Dioxasiliranes and Sila-Ureas Stable at Room Temperature. *Nat. Chem.* **2010**, *2*, 577.

(50) Muraoka, T.; Abe, K.; Haga, Y.; Nakamura, T.; Ueno, K. Synthesis of a Base-Stabilized Silanone-Coordinated Complex by Oxygenation of a (Silyl)(silylene)tungsten Complex. *J. Am. Chem. Soc.* **2011**, *133*, 15365.

(51) Rodriguez, R.; Gau, D.; Troadec, T.; Saffon-Merceron, N.; Branchadell, V.; Baceiredo, A.; Kato, T. A Base-Stabilized Sila-*β*-Lactone and a Donor/Acceptor-Stabilized Silanoic Acid. *Angew. Chem.* **2013**, *125*, 9150.

(52) Hannah, D. C.; Yang, J.; Kramer, N. J.; Schatz, G. C.; Kortshagen, U. R.; Schaller, R. D. Ultrafast Photoluminescence in Quantum-Confined Silicon Nanocrystals Arises from an Amorphous Surface Layer. *ACS Photonics* **2014**, *1*, 960.

(53) Kůsová, K.; Ondič, L.; Pelant, I. Comment on "Ultrafast Photoluminescence in Quantum-Confined Silicon Nanocrystals Arises from an Amorphous Surface Layer". *ACS Photonics* **2015**, *2*, 454−455.

(54) Hannah, D. C.; Yang, J.; Kramer, N. J.; Schatz, G. C.; Kortshagen, U. R.; Schaller, R. D. Reply to "Comment on 'Ultrafast Photoluminescence in Quantum-Confined Silicon Nanocrystals Arises from an Amorphous Surface Layer'". *ACS Photonics* **2015**, *2*, 456−458.

(55) Hessel, C. M.; Henderson, E. J.; Veinot, J. G. C. Hydrogen Silsesquioxane: A Molecular Precursor for Nanocrystalline Si−SiO$_2$ Composites and Freestanding Hydride-Surface-Terminated Silicon Nanoparticles. *Chem. Mater.* **2006**, *18*, 6139.

(56) Boukherroub, R.; Morin, S.; Wayner, D. D. M.; Bensebaa, F.; Sproule, G. I.; Baribeau, J. M.; Lockwood, D. J. Ideal Passivation of Luminescent Porous Silicon by Thermal, Noncatalytic Reaction with Alkenes and Aldehydes. *Chem. Mater.* **2001**, *13*, 2002.

(57) Sieval, A. B.; van den Hout, B.; Zuilhof, H.; Sudhölter, E. J. R. Molecular Modeling of Alkyl Monolayers on the Si(111) Surface. *Langmuir* **2000**, *16*, 2987.

(58) Sieval, A. B.; van den Hout, B.; Zuilhof, H.; Sudhölter, E. J. R. Molecular Modeling of Covalently Attached Alkyl Monolayers on the Hydrogen-Terminated Si(111) Surface. *Langmuir* **2001**, *17*, 2172.

(59) Kelly, J. A.; Shukaliak, A. M.; Fleischauer, M. D.; Veinot, J. G. C. Size-Dependent Reactivity in Hydrosilylation of Silicon Nanocrystals. *J. Am. Chem. Soc.* **2011**, *133*, 9564.

(60) Hessel, C. M.; Henderson, E. J.; Kelly, J. A.; Cavell, R. G.; Sham, T.-K.; Veinot, J. G. C. Origin of Luminescence from Silicon Nanocrystals: a Near Edge X-ray Absorption Fine Structure (NEXAFS) and X-ray Excited Optical Luminescence (XEOL) Study of Oxide-Embedded and Free-Standing Systems. *J. Phys. Chem. C* **2008**, *112*, 14247.

(61) Yang, Z.; Iqbal, M.; Dobbie, A. R.; Veinot, J. G. C. Surface-Induced Alkene Oligomerization: Does Thermal Hydrosilylation Really Lead to Monolayer Protected Silicon Nanocrystals? *J. Am. Chem. Soc.* **2013**, *135*, 17595.

(62) Wallart, X.; Henry de Villeneuve, C.; Allongue, P. Truly Quantitative XPS Characterization of Organic Monolayers on Silicon: Study of Alkyl and Alkoxy Monolayers on H−Si(111). *J. Am. Chem. Soc.* **2005**, *127*, 7871.

(63) Nemanick, E. J.; Hurley, P. T.; Brunschwig, B. S.; Lewis, N. S. Chemical and Electrical Passivation of Silicon (111) Surfaces through Functionalization with Sterically Hindered Alkyl Groups. *J. Phys. Chem. B* **2006**, *110*, 14800.

(64) Bansal, A.; Li, X.; Lauermann, I.; Lewis, N. S.; Yi, S. I.; Weinberg, W. H. Alkylation of Si Surfaces Using a Two-Step Halogenation/Grignard Route. *J. Am. Chem. Soc.* **1996**, *118*, 7225.

(65) Mason, M. D.; Credo, G. M.; Weston, K. D.; Buratto, S. K. Luminescence of Individual Porous Si Chromophores. *Phys. Rev. Lett.* **1998**, *80*, 5405.

(66) Sychugov, I.; Fucikova, A.; Pevere, F.; Yang, Z.; Veinot, J. G. C.; Linnros, J. Ultranarrow Luminescence Linewidth of Silicon Nanocrystals and Influence of Matrix. *ACS Photonics* **2014**, *1*, 998.

(67) Brus, L. E. A Simple Model for the Ionization Potential, Electron Affinity, and Aqueous Redox Potentials of Small Semiconductor Crystallites. *J. Chem. Phys.* **1983**, *79*, 5566.

(68) Brus, L. E. Electron−Electron and Electron−Hole Interactions in Small Semiconductor Crystallites: The Size Dependence of the Lowest Excited Electronic State. *J. Chem. Phys.* **1984**, *80*, 4403.

(69) Brus, L. Squeezing Light from Silicon. *Nature* **1991**, *353*, 301.

(70) Kontkiewicz, A. J.; Kontkiewicz, A. M.; Siejka, J.; Sen, S.; Nowak, G.; Hoff, A. M.; Sakthivel, P.; Ahmed, K.; Mukherjee, P.; Witanachchi, S.; Lagowski, J. Evidence that Blue Luminescence of Oxidized Porous Silicon Originates from SiO$_2$. *Appl. Phys. Lett.* **1994**, *65*, 1436.

(71) Anedda, A.; Bongiovanni, G.; Cannas, M.; Congiu, F.; Mura, A.; Martini, M. A 1.9 eV Photoluminescence Induced by 4 eV Photons in High-Purity Wet Synthetic Silica. *J. Appl. Phys.* **1993**, *74*, 6993.

(72) Fuzell, J.; Thibert, A.; Atkins, T. M.; Dasog, M.; Busby, E.; Veinot, J. G. C.; Kauzlarich, S. M.; Larsen, D. S. Red States versus Blue States in Colloidal Silicon Nanocrystals: Exciton Sequestration into Low-Density Traps. *J. Phys. Chem. Lett.* **2013**, *4*, 3806.

(73) Hao, X. J.; Podhorodecki, A. P.; Shen, Y. S.; Zatryb, G.; Misiewicz, J.; Green, M. A. Effects of Si-Rich Oxide Layer Stoichiometry on the Structural and Optical Properties of Si QD/ SiO$_2$ Multilayer Films. *Nanotechnology* **2009**, *20*, 485703.

(74) He, G. S.; Zheng, Q.; Yong, K.-T.; Erogbogbo, F.; Swihart, M. T.; Prasad, P. N. Two- and Three-Photon Absorption and Frequency Upconverted Emission of Silicon Quantum Dots. *Nano Lett.* **2008**, *8*, 2688.

(75) Sykora, M.; Mangolini, L.; Schaller, R. D.; Kortshagen, U.; Jurbergs, D.; Klimov, V. I. Size-Dependent Intrinsic Radiative Decay Rates of Silicon Nanocrystals at Large Confinement Energies. *Phys. Rev. Lett.* **2008**, *100*, 067401.

(76) Cicero, R. L.; Linford, M. R.; Chidsey, C. E. D. Photoreactivity of Unsaturated Compounds with Hydrogen-Terminated Silicon(111). *Langmuir* **2000**, *16*, 5688.

(77) Effenberger, F.; Götz, G.; Bidlingmaier, B.; Wezstein, M. Photoactivated Preparation and Patterning of Self-Assembled Monolayers with 1-Alkenes and Aldehydes on Silicon Hydride Surfaces. *Angew. Chem., Int. Ed.* **1998**, *37*, 2462.

(78) Sun, Q.-Y.; de Smet, L. C. P. M.; van Lagen, B.; Giesbers, M.; Thüne, P. C.; van Engelenburg, J.; de Wolf, F. A.; Zuilhof, H.; Sudhölter, E. J. R. Covalently Attached Monolayers on Crystalline Hydrogen-Terminated Silicon: Extremely Mild Attachment by Visible Light. *J. Am. Chem. Soc.* **2005**, *127*, 2514.

(79) Lauerhaas, J. M.; Credo, G. M.; Heinrich, J. L.; Sailor, M. J. Reversible Luminescence Quenching of Porous Silicon by Solvents. *J. Am. Chem. Soc.* **1992**, *114*, 1911.

(80) Fisher, D. L.; Gamboa, A.; Harper, J.; Lauerhaas, J. M.; Sailor, M. J. Photoluminescence Quenching of Porous Silicon. *MRS Proc.* **1994**, *358*, 507.

(81) Sailor, M. J.; Lee, E. J. Surface Chemistry of Luminescent Silicon Nanocrystallites. *Adv. Mater.* **1997**, *9*, 783.

(82) Klimov, V. I.; Schwarz, Ch. J.; McBranch, D. W.; White, C. W. Initial Carrier Relaxation Dynamics in Ion-Implanted Si Nanocrystals: Femtosecond Transient Absorption Study. *Appl. Phys. Lett.* **1998**, *73*, 2603.

(83) Lockwood, R.; Meldrum, A. Luminescence Simulations of Ensembles of Silicon Nanocrystals. *Phys. Status Solidi A* **2009**, *206*, 965.

(84) Belyakov, V. A.; Burdov, V. A.; Lockwood, R.; Meldrum, A. Silicon Nanocrystals: Fundamental Theory and Implications for Stimulated Emission. *Adv. Opt. Technol.* **2008**, *2008*, 32.